Hepatocellular Carcinoma: Hepatocyte-selective Enhancement at Gadoxetic Acid–enhanced MR Imaging—Correlation with Expression of Sinusoidal and Canalicular Transporters and Bile Accumulation[1]

Takahiro Tsuboyama, MD
Hiromitsu Onishi, MD, PhD
Tonsok Kim, MD, PhD
Hirofumi Akita, MD
Masatoshi Hori, MD, PhD
Mitsuaki Tatsumi, MD, PhD
Atsushi Nakamoto, MD
Hiroaki Nagano, MD, PhD
Nariaki Matsuura, MD, PhD
Kenichi Wakasa, MD, PhD
Kaname Tomoda, MD, PhD

Purpose: To investigate the mechanism of enhancement of hepatocellular carcinoma (HCC) on gadoxetic acid–enhanced hepatobiliary phase magnetic resonance (MR) images and to characterize HCC thus enhanced.

Materials and Methods: This retrospective study was approved by the institutional review board, and patient informed consent for research use of the resected specimen was obtained. MR images in 25 patients (20 men, five women; mean age, 68 years; range, 49–82 years) with 27 resected hypervascular HCCs (one well, 13 moderately, 13 poorly differentiated) that demonstrated hepatocyte-selective enhancement on gadoxetic acid–enhanced MR images, were quantitatively studied, and findings were correlated with results of immunohistochemical staining for a sinusoidal transporter, organic anion transporting polypeptide (OATP) 1B1 (OATP1B1) and/or OATP1B3 (OATP1B1 and/or -1B3), and a canalicular transporter, multidrug resistance–associated protein 2 (MRP2), and also with bile accumulation in tumors. Statistical analysis was performed with the Student *t* test and Scheffé post hoc test.

Results: Combined with positive OATP1B1 and/or -1B3 expression (O+), two patterns of MRP2 expression contributed to high enhancement: decreased expression (M−, $n = 3$) and increased expression at the luminal membrane of pseudoglands (M+[P], $n = 3$). Nodules without OATP1B1 and/or -1B3 expression (O−, $n = 13$) and nodules with O+ associated with increased MRP2 expression only at the canaliculi (M+[C], $n = 8$) induced significantly lower enhancement than those with the two expression patterns described before (O+/M− group vs O− group, $P = .002$; O+/M− group vs O+/M+[C] group, $P = .047$; O+/M+[P] group vs O− group, $P < .001$; O+/M+[P] group vs O+/M+[C] group, $P < .001$). Nodules with bile pigment ($n = 12$) showed significantly higher enhancement ($P = .004$); all five nodules (one well differentiated HCC, four moderately differentiated HCCs), which were enhanced more than adjacent liver parenchyma, contained bile pigment.

Conclusion: High hepatocyte-selective enhancement is induced by expression patterns of transporters, which may result in accumulation of gadoxetic acid in cytoplasm of tumor cells or in lumina of pseudoglands. An HCC with gadoxetic acid enhancement is characterized by bile accumulation in tumors.

Supplemental material: *http://radiology.rsna.org/lookup/suppl/doi:10.1148/radiol.10091557/-/DC1*

[1] From the Departments of Radiology (T.T., H.O., T.K., M.H., M.T., A.N., K.T.) and Surgery (H.A., H.N.), Osaka University Graduate School of Medicine, 2-2 Yamadaoka, Suita, Osaka 565-0871, Japan; Department of Molecular Pathology, Osaka University Graduate School of Medicine and Health Science, Osaka, Japan (N.M.); and Department of Pathology, Osaka City University Hospital, Osaka, Japan (K.W.). Received August 20, 2009; revision requested October 6; final revision received November 12; accepted December 16; final version accepted January 11, 2010. **Address correspondence to** T.T. (e-mail: *t-tsuboyama@radiol.med.osaka-u.ac.jp*).

Gadoxetic acid is a newly developed liver-specific contrast agent for magnetic resonance (MR) imaging (1). This agent is characterized by combined good extracellular and hepatocyte-selective properties (2). Approximately 50% of the administered dose is taken up by hepatocytes and excreted into bile, and this rate is much higher than the hepatic uptake of another liver-specific contrast agent, gadobenate dimeglumine (3). As a result of the hepatic uptake, maximal enhancement of normal liver parenchyma is obtained in the hepatobiliary phase, about 20 minutes after injection of gadoxetic acid (4), which thus allows for improved detection of focal liver lesions that lack functioning hepatocytes (2,5–7).

Positive enhancement at gadoxetic acid–enhanced hepatobiliary phase imaging occurs not only in normal liver parenchyma but also in focal liver lesions of hepatocellular origin, such as focal nodular hyperplasia (8,9). Some investigators have reported that positive hepatocyte-selective enhancement may also be observed in some patients with hepatocellular carcinoma (HCC) (7,8,10–12). This seemingly paradoxical enhancement of HCC was limited to well-differentiated HCC in some studies (8,11), whereas it was also observed in moderately or poorly differentiated HCC in other studies (7,10,12). However, little is known about the mechanism of this enhancement of HCC or about the characteristics of HCC thus enhanced.

It has been suggested that organic anion transporting polypeptides (OATPs), expressed at the basolateral membrane of hepatocytes, mediate the uptake of gadoxetic acid (13) and that multidrug resistance-associated protein 2 (MRP2), expressed in the canalicular membrane, mediates the secretion from hepatocytes (14). Of the OATP family, rat Oatp1a1 was demonstrated to be a carrier of gadoxetic acid, whereas human OATP1A2 was not involved in its uptake (15). This finding was followed by cloning of the most dominant OATPs in human liver, OATP1B1 and OATP1B3 (16,17), which are now considered promising candidates as potential transporters of gadoxetic acid in human liver.

Some investigators (10,18–22) have reported that HCC tumor cells expressed the hepatocellular transporters, including OATP1B1 and/or OATP1B3 (hereafter, OATP1B1 and/or -1B3) and MRP2. We therefore hypothesized that the degree of expression of these transporters in tumor cells may affect the kinetics of gadoxetic acid in tumors.

The purpose of this study was to investigate the mechanism of enhancement of HCC on gadoxetic acid–enhanced hepatobiliary phase MR images and to characterize HCC thus enhanced.

Advances in Knowledge

- Expression of a sinusoidal transporter, organic anion transporting polypeptide 1B1 (OATP1B1) and/or OATP1B3 (OATP1B1 and/or -1B3), is essential but not sufficient for high hepatocyte-selective enhancement of hepatocellular carcinoma (HCC) on gadoxetic acid–enhanced MR images, because all nodules with high enhancement showed positive expression of OATP1B1 and/or -1B3, whereas 64% of nodules with positive OATP1B1 and/or -1B3 expression demonstrated low enhancement.
- Combined with OATP1B1 and/or -1B3 expression, two expression patterns of a canalicular transporter, multidrug resistance–associated protein 2, contributed to high enhancement, a decreased expression and an increased expression at the luminal membrane of pseudoglands.
- HCC with high hepatocyte-selective enhancement is characterized by bile accumulation in tumors.

Implication for Patient Care

- HCC with bile accumulation should be included in the differential diagnosis for tumors with positive enhancement on gadoxetic acid–enhanced hepatobiliary phase MR images.

Materials and Methods

Patients

Institutional review board approval for this retrospective study was obtained from Osaka University Hospital (Osaka, Japan), and written informed consent for research use of the resected specimen was obtained from all patients. The surgery, pathology, and radiology records of patients with HCC who underwent surgery at our institution between April 1, 2008, and June 30, 2009, were reviewed. Inclusion criteria were preoperative gadoxetic acid–enhanced MR examination and presence of histopathologically proved nodular HCC at surgery. Forty-eight patients with 50 HCCs that were histopathologically proved by surgical resection were identified; 42 of these patients had undergone preoperative gadoxetic acid–enhanced MR examination within 2 months of the surgical procedure. Exclusion criteria included preoperative treatment, such as transcatheter arterial chemoembolization, and the presence of abnormal signal intensity (SI) in liver parenchyma adjacent to the tumor on MR images, because the correlation

Published online
10.1148/radiol.10091557

Radiology 2010; 255:824–833

Abbreviations:
HBV = hepatitis B virus
HCC = hepatocellular carcinoma
HCV = hepatitis C virus
MRP = multidrug resistance–associated protein
OATP = organic anion transporting polypeptide
ROI = region of interest
SI = signal intensity

Author contributions:
Guarantors of integrity of entire study, T.T., T.K.; study concepts/study design or data acquisition or data analysis/interpretation, all authors; manuscript drafting or manuscript revision for important intellectual content, all authors; approval of final version of submitted manuscript, all authors; literature research, T.T., H.O., M.H.; clinical studies, T.T., H.O., T.K., H.A., M.H., M.T., A.N., H.N., N.M., K.W.; statistical analysis, T.T.; and manuscript editing, T.T., H.O., T.K., K.T.

Authors stated no financial relationship to disclose.

Table 1

Summary of Relative Enhancement Ratios, Expression of Transporters, and Bile Pigment Findings

Patient No.*	Child-Pugh Class	Cause	Background Liver	Tumor Grade†	Tumor Size (mm)	Relative Enhancement Ratio	OATP1B1 and/or -1B3 Expression Score‡	MRP2 Expression Score ‡		Bile Pigment Score and Location#
								Canaliculus§	Pseudogland‖	
					Nodules with High Enhancement **					
1	A	HCV	Chronic hepatitis	M	25	1.48	1+	2+	2+	2+, pseudogland
2	A	HCV	Cirrhosis	W	14	1.39	2+	2+	2+	1+, pseudogland
3	B	HCV	Cirrhosis	M	28	1.13	2+	1+	NCS	2+, cytoplasm
4	A	Alcohol	Chronic hepatitis	M	27	1.13	2+	1+	1+	1+, cytoplasm
5	A	HCV	Chronic hepatitis	M	15	1.05	1+	2+	2+	1+, pseudogland
					Nodules with Low Enhancement††					
6	B	Unknown	Normal	M	29	0.86	0	NCS	2+	0
7	A	HCV	Cirrhosis	P	31	0.84	2+	2+	1+	1+, ND
8	A	HBV	Cirrhosis	P	30	0.84	1+	2+	1+	0
9	B	HCV	Cirrhosis	P	16	0.80	1+	2+	NCS	0
3	B	HCV	Cirrhosis	M	30	0.80	1+	2+	NCS	1+, cytoplasm
10	A	HCV	Cirrhosis	M	23	0.79	1+	1+	NCS	0
11	A	HBV	Chronic hepatitis	P	35	0.78	1+	2+	0	1+, pseudogland
12	A	HCV	Chronic hepatitis	M	15	0.78	1+	2+	NCS	0
13	B	HCV	Cirrhosis	P	13	0.78	0	2+	NCS	1+, ND
14	A	HCV	Cirrhosis	P	33	0.77	0	1+	1+	0
15	B	HBV	Cirrhosis	M	24	0.76	0	2+	1+	1+, cytoplasm
16	A	HBV	Cirrhosis	P	17	0.71	0	2+	NCS	0
17	A	HBV	Chronic hepatitis	P	30	0.70	2+	2+	0	0
18	A	HCV	Chronic hepatitis	M	10	0.69	0	2+	2+	1+, ND
19	A	HCV	Cirrhosis	P	17	0.69	0	2+	1+	0
20	A	HBV	Chronic hepatitis	M	37	0.66	0	2+	2+	0
21	A	Unknown	Normal	P	58	0.66	0	1+	0	0
22	A	HBV	Chronic hepatitis	M	18	0.65	1+	2+	NCS	0
23	A	HCV	Cirrhosis	P	10	0.64	0	1+	NCS	0
24	B	HCV	Cirrhosis	P	25	0.63	0	2+	0	1+, ND
19	A	HCV	Cirrhosis	P	21	0.52	0	1+	NCS	0
25	A	HBV	Chronic hepatitis	M	32	0.52	0	2+	0	0

* Patients are listed in descending order of values of relative enhancement ratios. Two nodules were assessed separately in patients 3 and 19.

† M = moderately differentiated HCC, W = well-differentiated HCC, P = poorly differentiated HCC.

‡ 0 = negative or minimal, 1+ = positive to the same or lesser extent than the liver parenchyma, 2+ = positive to a greater extent compared with liver parenchyma, NCS = no corresponding structure.

§ Expression at canalicular membrane of trabecular structure.

‖ Expression at luminal membrane of pseudoglandular structure.

The location of bile pigment was determined at microscopic examination. 0 = negative, 1+ = focal, 2+ = diffuse, ND = not detected.

** High enhancement = relative enhancement ratio greater than one.

†† Low enhancement = relative enhancement ratio less than one.

between the histopathologic and imaging findings and the comparison between the SI of the tumors and the SI of adjacent liver parenchyma were difficult. A total of 17 of 42 patients were excluded; 14 patients with 16 HCCs who underwent preoperative transcatheter arterial chemoembolization and three patients with three HCCs (two patients with recurrent tumor near the site of previous surgery and one patient with portal vein tumor thrombus) with abnormal SI in the adjacent liver parenchyma. Two HCCs included in this study consisted of two distinct nodules with different SI on contrast material–enhanced MR images (Table 1, patients 3 and 19), and each nodule was assessed separately. Finally, 25 patients with 27 HCC nodules were included in this study.

The patients ranged from 49 to 82 years of age (mean, 68 years). Twenty patients were men (mean age, 68 years; range, 49–82 years), and five were women (mean age, 70 years; range, 63–78 years). Thirteen patients had underlying liver cirrhosis and nine had chronic hepatitis, caused by hepatitis B virus (HBV) in eight patients and hepatitis C virus (HCV) in 14 patients. One patient had alcoholic chronic hepatitis, and two had a normal liver. In these patients, liver function was based on the

Table 2

Summary of the MR Examination

A: Liver Acquisition with Volume Acceleration Sequence	
Parameter	Value*
Repetition time (msec)	4.5/3.6
Echo time (msec)	2.2/1.7
Flip angle (degree)	12/12
Inversion time (msec)	7/5
Bandwidth (kHz)	62.5/83.8
Matrix	320 × 192/320 × 192
Field of view (mm)	340/340
Section thickness (mm)	4/4
Array spatial sensitivity-encoding technique factor	2/2
B: Gadoxetic Acid-enhanced Imaging Method	
Feature	Administration
Dose of gadoxetic acid	0.025 mmol per kilogram of body weight
Image delay	
For arterial phase	10 sec after triggering†
For portal venous phase	70 sec after injection
For equilibrium phase	180 sec after injection
For hepatobiliary phase	20 min after injection

Note.—All images were obtained in transverse plane.

* Data are values for 1.5-T system/3-T system.

† Triggering = the arrival of contrast material at the abdominal aorta.

Child-Pugh classification: In 19 patients, nodules were categorized as class A, and in six patients, nodules were categorized as class B. Tumors ranged in size from 10 to 58 mm (mean, 25 mm). All nodules were hypervascular tumors, showing hyperenhancement relative to the surrounding liver parenchyma in the arterial phase of the dynamic MR examination.

MR Examination

The MR examinations were performed with a 1.5-T MR system (Signa Excite HD; GE Healthcare, Milwaukee, Wis) in nine patients and with a 3-T system (Signa HDx; GE Healthcare) in the other 16 patients. An eight-channel phased-array coil system for the abdominopelvic region was used.

Images were obtained by using a breath-hold T1-weighted three-dimensional gradient-echo sequence (liver acquisition with volume acceleration, or LAVA) with fat suppression as follows: at imaging before administration of contrast agent, at dynamic triple-phase imaging after administration of gadoxetic acid (Primovist; Bayer-Schering Pharma AG, Berlin, Germany), and at hepatobiliary phase imaging. The parallel imaging technique (array spatial sensitivity encoding technique, or ASSET) also was used. The method for the MR examination is summarized in Table 2. Hepatobiliary phase imaging was performed 20 minutes after injection of contrast agent.

Histopathologic Analysis

Four-micrometer-thick tissue sections prepared from formalin-fixed paraffin-embedded blocks were stained with hematoxylin-eosin and were reviewed by two authors (K.W. and N.M., with 28 and 18 years of experience, respectively) who specialize in liver pathology. Histopathologic grading was determined according to criteria proposed previously (23–25). One nodule was classified as a well-differentiated HCC, 13 were classified as moderately differentiated HCCs, and 13 were classified as poorly differentiated HCCs. Pseudoglandular structures of various numbers and sizes were found in 17 nodules, and one of the tumors consisted of only pseudoglandular structures.

Immunohistochemical Staining

Immunohistochemical staining of tumors and the adjacent liver parenchyma was performed with a staining kit (Vectastain ABC Peroxidase Kit; Vector Laboratories, Burlingame, Calif) for OATP1B1 and/or -1B3 and MRP2 on 3.5-μm-thick, formalin-fixed, paraffin-embedded sections. Autoclave antigen retrieval in 10 mmol/L citrate buffer (pH 6.0) was performed, followed by endogenous peroxidase activity blocking with a 1% H_2O_2 solution in methanol. Serum blocking was performed by using 10% normal horse serum. The sections were incubated at 4°C overnight with primary monoclonal antibodies against OATP1B1 and/or -1B3 (clone mMDQ, 1:100) (Progen Biotechnik, Heidelberg, Germany) and MRP2 (clone M2III-6, 1:50) (Monosan, Uden, the Netherlands). Secondary biotinylated anti-mouse antibody (BA2000; Vector Laboratories) was used at a dilution of 1:100 at room temperature. The immunopositivity was visualized by means of 3,3′-diaminobenzidine. Sections were counterstained with hematoxylin.

Evaluation of MR Images

MR images were reviewed by two abdominal radiologists (H.O. and T.K., with 12 and 19 years of experience, respectively) who specialized in hepatic MR imaging. Quantitative analysis for tumor enhancement at hepatobiliary phase imaging was performed by the following method (26). First, the SI of tumors and the SI of the adjacent liver parenchyma were measured in regions of interest (ROIs) placed on precontrast and postcontrast hepatobiliary phase MR images. The two radiologists placed all ROIs at the section level of the largest tumor diameter devoid of necrosis in consensus. Tumor ROIs were determined by tracing the margin of the tumor, even though the SI was heterogeneous in each of the ROIs devoid of necrosis (mean ROI, 336 mm^2; range, 72–807 mm^2). ROIs on the adjacent liver parenchyma were determined by tracing the surrounding nontumorous region approximately within 20 mm from the tumor while avoiding vascular structures (mean ROI, 904 mm^2; range, 268–2544 mm^2).

Next, the relative intensity ratio was calculated on precontrast and postcontrast MR images, with the following formula: RIR = SI_{nod}/SI_{par}, where RIR is the relative intensity ratio, SI_{nod} is the SI of the nodule, and SI_{par} is the SI of the liver parenchyma. The enhancement of nodules compared with that of the liver parenchyma was defined as the relative enhancement ratio of nodules and was calculated with the following formula: RER = RIR_{post}/RIR_{pre}, where RER is the relative enhancement ratio, RIR_{post} is the postcontrast relative intensity ratio, and RIR_{pre} is the precontrast relative intensity ratio. Tumor enhancement was defined as high when the relative enhancement ratio was more than one, which meant that the tumor was enhanced more than the adjacent liver parenchyma, and as low when the relative enhancement ratio was less than one.

Evaluation of Immunohistochemical Staining Results

Immunostaining of the tumors and that of the adjacent liver parenchyma was compared in terms of staining patterns and stain intensities by the two previously described liver pathologists, independently and without knowledge of the MR imaging data. Disagreement was resolved with consensus. The results of immunohistochemical staining for tumors were determined by using the following three-point scale: score 0, negative or minimal; score 1+, positive to the same or lesser extent compared with the adjacent liver parenchyma; and score 2+, positive to a higher degree than the adjacent liver parenchyma (Figs E1, E2 [online]). Immunopositivity was determined by staining of the membrane of hepatocytes or tumor cells but not in terms of cytoplasmic reactivity, if present. MRP2 expression in tumors was assessed separately on canaliculi and the luminal membrane of pseudoglands.

Evaluation of Bile Pigment

The degree and the location of bile pigment of HCC were evaluated macroscopically on color images of the cut surface of the resected specimens and microscopically on sections stained with hematoxylin-eosin by means of its greenish color. Two authors (H.A. and K.W., with 8 years of experience in hepatobiliary surgery and 28 years experience in liver pathology, respectively) rated the degree of bile accumulation in consensus with the following three-point scale: score 0, negative; score 1+, focal; and score 2+, diffuse.

Statistical Analysis

In regard to statistical analysis of OATP1B1 and/or -1B3 and bile pigment, categories 1+ and 2+ were combined, although the evaluation data were collected on a three-point scale. In regard to statistical analysis of MRP2, overall expression was determined by combining the results for expression on canaliculi and pseudoglands. When the degrees of expression on the two structures were the same, the same score was assigned for the overall expression, and when the degrees of expression on the two structures were different, the higher score was applied as the overall expression. The Student *t* test was then used to compare the relative enhancement ratio between the two groups, specifically for the following: nodules with positive (score 1+ or 2+) versus negative or minimal (score 0) expression of OATP1B1 and/or -1B3, nodules with increased (score 2+) versus decreased (score 1+) overall expression of MRP2, and nodules with present (score 1+ or 2+) versus absent (score 0) bile pigment. Tumor sizes were also compared between nodules with high and low enhancement by using the Student *t* test. An analysis of variance was used for multigroup comparison, and when the results showed significant differences among groups, comparisons between groups were performed with the Scheffé post hoc test. A *P* value of less than .05 was considered to indicate a significant difference.

Results

Expression of OATP1B1 and/or -1B3

Basolateral expression in liver parenchyma was strong in the centrilobular area, moderate in the midzonal area, and absent in periportal hepatocytes (Fig E1a [online]), which is in agreement with the data in previous studies (18,19). Positive expression of OATP1B1 and/or -1B3 in HCC was observed in 14 (52%) nodules. The distribution of positive cells was broad and diffuse (Fig E1b [online]) in five nodules and focal and sparse (Fig E1c [online]) in nine nodules.

Expression of MRP2

Canalicular expression of MRP2 without zonal variation was observed in liver parenchyma (Fig E2a [online]). All HCC nodules were positive for MRP2, and the expression was localized either in the luminal membrane of pseudoglands (Fig E2b [online]) or in the canalicular membrane of tumor cells arranged in trabecular structures (Fig E2c, E2d [online]). Overall MRP2 expression was increased in 20 (74%) nodules and unchanged or decreased in seven (26%) nodules. Of the 20 nodules with increased expression, six nodules showed increased expression at the luminal membrane of the pseudoglands (Fig E2b [online]), and the remaining 14 nodules showed increased expression only at the canaliculi and decreased or negative expression in the luminal membrane of pseudoglands, if present (Fig E2c [online]).

Relative Enhancement Ratio of Tumors in Relation to Expression of Transporter Proteins and Bile Accumulation

The mean relative enhancement ratio for all nodules was 0.82. Nodules with positive expression of OATP1B1 and/or -1B3 showed a significantly higher relative enhancement ratio than did nodules with negative or minimal expression (mean, 0.94 and 0.68, respectively; $P = .002$) (Fig 1a). All five nodules with high enhancement expressed OATP1B1 and/or -1B3, whereas nine (64%) of 14 nodules with positive OATP1B1 and/or -1B3 expression showed low enhancement similar to that of the nodules with negative or minimal expression (Table 1). There was no significant difference in mean relative enhancement ratio between nodules with increased MRP2 expression and those with unchanged or decreased MRP2 expression (mean, 0.82 and 0.81, respectively; $P = .9$) (Fig 1b).

Radiology

Figure 1

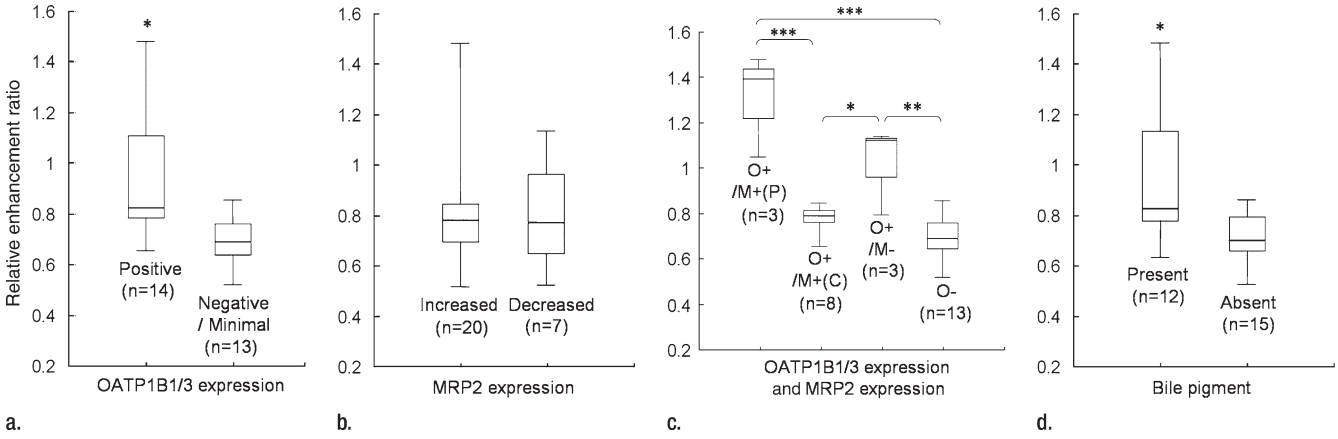

Figure 1: Box plots of relative enhancement ratios of nodules, indicating the median (horizontal line), the 75th (top of box) and 25th (bottom of box) quartiles, and the smallest and largest values (whiskers). **(a)** OATP1B1 and/or -1B3 expression. Mean values were significantly higher for nodules with positive expression than for nodules with negative or minimal expression. $* = P = .002$, Student *t* test. **(b)** MRP2 expression. Mean values were not significantly different for nodules with increased expression and nodules with unchanged or decreased expression ($P = .9$, Student *t* test). **(c)** OATP1B1 and/or -1B3 *(OATP1B1/3)* and MRP2 expression, with comparison of four groups of nodules classified by expression patterns of both OATP1B1 and/or -1B3 and MRP2. Mean values were significantly higher for the two groups: nodules with increased MRP2 expression at the luminal membrane of pseudoglands and nodules with decreased MRP2 expression, both combined with positive OATP1B1 and/or -1B3 expression (Scheffé post hoc test). $* = P = .047$, $** = P = .002$, $*** = P < .001$. *O+* = OATP1B1 and/or -1B3 positive, *O–* = OATP1B1 and/or -1B3 negative, *M+(P)* = increased MRP2 expression at luminal membrane of pseudoglands, *M+(C)* = increased MRP2 expression only at canaliculi, *M–* = unchanged or decreased MRP2 expression. **(d)** Bile pigment. Mean values were significantly higher for nodules with bile pigment than for nodules without bile pigment. $* = P = .004$, Student *t* test.

Figure 2

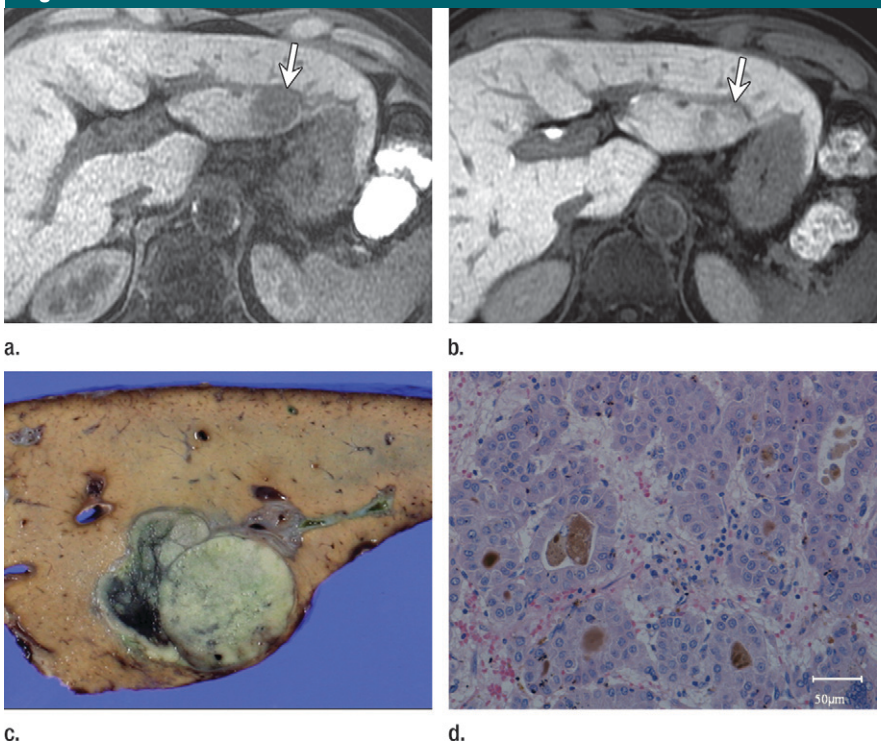

Figure 2: Moderately differentiated HCC with high hepatocyte-selective enhancement in 65-year-old man (Table 1, patient 1). **(a)** Precontrast MR image shows tumor (arrow, also on **b**). **(b)** Gadoxetic acid–enhanced hepatobiliary phase MR image shows that tumor had higher enhancement than did adjacent liver parenchyma. **(c)** Image shows that tumor had diffuse greenish color on cut surface. **(d)** Photomicrograph of section stained with hematoxylin-eosin shows bile pigment in lumina of pseudoglands. (Original magnification, ×20.) Immunohistochemical staining showed prominent expression of MRP2 in luminal membrane of pseudoglands (Fig E2b [online]). OATP1B1 and/or -1B3 expression was positive (not shown).

Figure 3

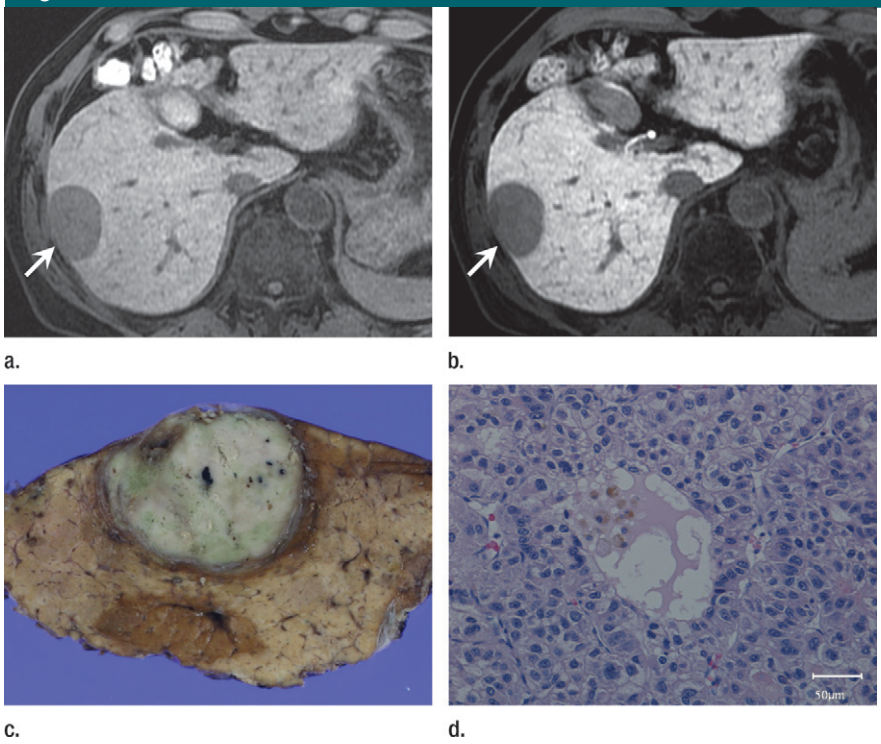

Figure 3: Poorly differentiated HCC with low hepatocyte-selective enhancement in 60-year-old man (Table 1, patient 11). **(a)** Precontrast MR image shows tumor (arrow, also on **b**). **(b)** Gadoxetic acid–enhanced hepatobiliary phase MR image shows that tumor was less enhanced than was adjacent liver parenchyma. **(c)** Image shows that tumor had focal greenish color on cut surface. **(d)** Photomicrograph of section stained with hematoxylin-eosin shows that bile pigment was localized in lumina of pseudoglands and was phagocytosed by macrophages. (Original magnification, ×20.) Immunohistochemical analysis demonstrated that MRP2 expression was increased in canalicular membrane but was minimal in luminal membrane of pseudoglands (Fig E2c [online]). OATP1B1 and/or -1B3 expression was positive (not shown).

Figure 4

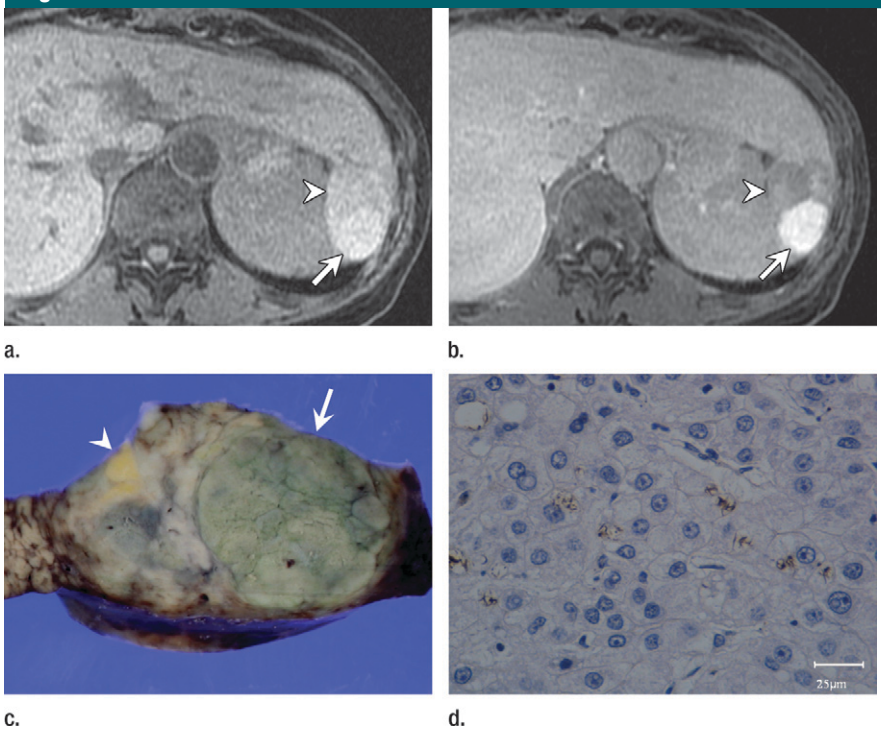

Figure 4: Moderately differentiated HCC (Table 1, patient 3) consisting of two nodules with different degrees of hepatocyte-selective enhancement in 67-year-old woman. **(a)** Precontrast MR image shows ventral nodule (arrowhead, also on **b** and **c**) and dorsal nodule (arrow, also on **b** and **c**). **(b)** Gadoxetic acid–enhanced hepatobiliary phase MR image, the ventral nodule was less enhanced, whereas the dorsal nodule was more enhanced than was the liver parenchyma. **(c)** Image shows that had greenish color on cut surface and was focal in ventral nodule and diffuse in dorsal nodule, which correlated well with the degree of tumor enhancement. **(d)** Photomicrograph of section stained with hematoxylin-eosin shows that bile pigment was found in cytoplasm of tumor cells of dorsal nodule. (Original magnification, ×40.) Dorsal nodule showed diffuse OATP1B1 and/or -1B3 expression (Fig E1b [online]) and decreased MRP2 expression (Fig E2d [online]); ventral nodule showed decreased OATP1B1 and/or -1B3 expression (Fig E1c [online]) and increased MRP2 expression at the canalicular membrane (not shown).

Figure 5

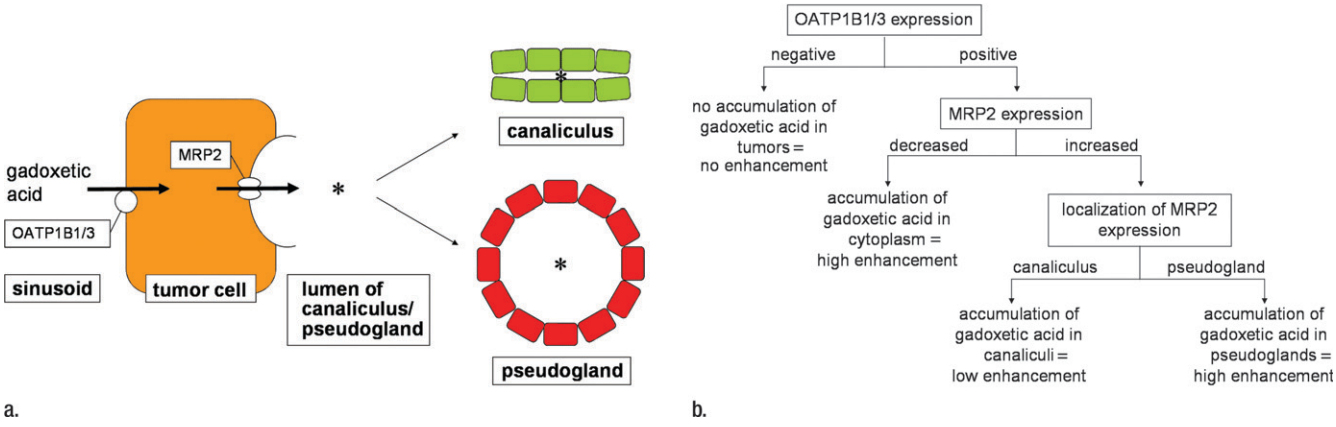

Figure 5: Hypothetical mechanism of gadoxetic acid accumulation in HCC. **(a)** Diagram shows that OATP1B1 and/or -1B3 *(OATP1B1/3)* mediates uptake of gadoxetic acid from sinusoid to tumor cell, whereas MRP2 mediates secretion of gadoxetic acid from tumor cell to lumen (*) of canaliculus or *(/)* pseudogland. **(b)** Flowchart illustrates relationship between transporter expression pattern and accumulation pattern of gadoxetic acid. Tumors without OATP1B1 and/or -1B3 expression do not accumulate gadoxetic acid, whereas tumors with OATP1B1 and/or -1B3 expression accumulate gadoxetic acid in cytoplasm, canaliculi, or pseudoglandular lumina, depending on MRP2 expression patterns.

Figure 1c shows relative enhancement ratios of the four groups classified by expression patterns of both OATP1B1 and/or -1B3 and MRP2: nodules with positive OATP1B1 and/or -1B3 expression associated with increased MRP2 expression at the luminal membrane of pseudoglands, O+/M+(P) group (Fig 2); nodules with positive OATP1B1 and/or -1B3 expression associated with increased MRP2 expression only at the canaliculi, O+/M+(C) group (Figs 3, 4); nodules with positive OATP1B1 and/or -1B3 expression associated with decreased MRP2 expression, O+/M− group (Fig 4); and nodules with negative or minimal OATP1B1 and/or -1B3 expression, O− group. The respective mean relative enhancement ratios were 1.31, 0.77, 1.02, and 0.68. The differences were significant among the four groups for the two groups with mean relative enhancement ratios higher than one and the other two groups with mean relative enhancement ratios lower than one (O+/M+[P] group vs O+/M+[C] group, $P < .001$; O+/M+[P] group vs O− group, $P < .001$; O+/M− group vs O+/M+[C] group, $P = .047$; O+/M− group vs O− group, $P = .002$).

Nodules with bile pigment showed significantly higher relative enhancement ratios than did nodules without bile pigment (mean, 0.96 and 0.71, respectively; $P = .004$) (Fig 1d).

Characteristics of Nodules with High Enhancement

Five nodules showed high enhancement (Table 1), all of which contained bile pigment. Tumors ranged in size from 14 to 28 mm, and there was no significant difference in size between nodules with high and low enhancement (mean, 22 and 25 mm, respectively; $P = .52$). Four of them were moderately differentiated HCCs and one was a well-differentiated HCC. Three of the five nodules expressed OATP1B1 and/or -1B3 moderately or strongly and MRP2 strongly in the luminal membrane of pseudoglands where the bile pigments had accumulated (Fig 2). The remaining two nodules expressed OATP1B1 and/or -1B3 strongly and MRP2 weakly both at the canaliculi and at the luminal membrane of pseudoglands in one nodule and only at the canaliculi in the other nodule, and bile pigment was observed in their cytoplasm (Fig 4).

Discussion

It has been reported that some HCCs, in spite of lacking normal hepatocytes, show positive hepatocyte-selective enhancement on gadoxetic acid–enhanced hepatobiliary phase MR imaging (11,12). Although the mechanism of this seemingly paradoxical tumor enhancement has not been fully elucidated, the findings of our study suggest that the degree of expression and the localization of OATP1B1 and/or -1B3 and MRP2 in tumors affect the degree of hepatocyte-selective enhancement of HCCs.

Positive OATP1B1 and/or -1B3 expression was associated with significantly higher hepatocyte-selective enhancement of HCCs, whereas tumor enhancement was not significantly different, whether the overall degree of MRP2 expression had increased or decreased. When considering the localization in addition to the degree of expression, two patterns of MRP2 expression then contributed to high tumor enhancement when combined with positive OATP1B1 and/or -1B3 expression; one was a decreased expression and the other was an increased expression at the luminal membrane of pseudoglands. All five nodules with high enhancement showed either of these two patterns of transporter expression. In contrast, increased MRP2 expression only at the canalicular membrane induced significantly lower enhancement than did the two expression patterns described

above, in spite of immunopositivity for OATP1B1 and/or -1B3.

On the basis of our results, we suggest that accumulation of gadoxetic acid in tumors is caused by the following three-step mechanism (Fig 5): In the first step, expression of OATP1B1 and/or -1B3 determines whether tumor cells take up gadoxetic acid. Consequently, gadoxetic acid does not accumulate in tumors without OATP1B1 and/or -1B3 expression. In the second step, expression of MRP2 determines whether tumor cells secrete gadoxetic acid. Gadoxetic acid consequently accumulates in the cytoplasm of tumor cells if MRP2 expression is decreased. In the third step, localization of increased MRP2 expression determines whether tumor cells secrete gadoxetic acid into the lumina of canaliculi or into pseudoglands, where secreted gadoxetic acid can be expected to accumulate because bile ducts are absent in moderately or poorly differentiated HCC (23,27,28). We speculated that the degree of enhancement was determined by the amount of accumulated gadoxetic acid, which would be larger in cytoplasm or in pseudoglandular lumina than in canaliculi because there is little space inside the latter.

In previous studies of transporter expression in HCC, results indicate that OATP1B1 and/or -1B3 expression seems to be generally reduced (18–21) and MRP2 expression, on the other hand, is generally maintained or even increased in HCC (22). These results are consistent with ours. Furthermore, we found that increased expression of MRP2 was common at the canalicular membrane but not at the luminal membrane of pseudoglands. All these results can explain why HCC generally shows low hepatocyte-selective enhancement on gadoxetic acid–enhanced MR images. Changes in these transporter activities during hepatocarcinogenesis, which might be accompanied by changes in hepatocyte-selective enhancement of tumors, have not yet been clarified.

In our study, all five nodules with high enhancement accumulated bile pigment. In addition, bile pigment was often observed in the area where we expected gadoxetic acid to accumulate. The greenish color derives from bilirubin (29), and bilirubin transport is reportedly mediated by OATP1B1 and MRP2 (30,31). It is, therefore, likely that bilirubin and gadoxetic acid show similar distribution patterns in tumors. However, some green hepatomas showed low enhancement. This discrepancy may be owing to the fact that the substrate specificity differs slightly between OATP1B1 and OATP1B3 (16,17,30). In fact, OATP1B3 has been suggested to be a key transporter for gadoxetic acid uptake (10) but not for bilirubin (30). Another possible reason is that persistent retention of birilubin may be observed in tumors that have already lost their transporting ability. This bile pigment may disappear gradually while it is being phagocytosed by macrophages.

As for tumor grading, positive hepatocyte-selective enhancement has been reported in all grades of tumors (7,8,10–12). In our study, one well-differentiated HCC and four moderately differentiated HCCs showed high enhancement, whereas no poorly differentiated HCC demonstrated high enhancement. Further evaluation is needed to determine the relationship, if any, between tumor grade and hepatocyte-selective enhancement.

There were some limitations in our study. First, the study population was small, including only five tumors with high hepatocyte-selective enhancement. Second, this study could not avoid sampling bias because of its retrospective design. Third, we used relative enhancement ratios to evaluate the degree of tumor enhancement, which might also be affected by hepatic parenchymal enhancement. We, therefore, evaluated the transporter expression in tumors in a manner that was similar to the manner used for the evaluation of tumor enhancement, by comparing expression in tumors with that in adjacent liver parenchyma. Furthermore, in this study population, liver function, which affects the hepatic enhancement (32), was good enough to allow liver resection. This factor will not be the case in all liver tumors. Last, we did not exclude certain additional factors that might affect kinetics of gadoxetic acid in tumors. There are many other transporters expressed at the basolateral or canalicular membrane of hepatocytes (33), and their involvement in gadoxetic acid transport remains to be evaluated.

In conclusion, our results suggest that expression of OATP1B1 and/or -1B3 in tumor cells is essential but not sufficient for hepatocyte-selective enhancement of HCC and that high enhancement is induced either by decreased expression of MRP2 in tumor cells or by increased expression of MRP2 at the luminal membrane of pseudoglands, which we speculated may have resulted in accumulation of gadoxetic acid in the cytoplasm of tumor cells or in the lumina of pseudoglands. HCC with high hepatocyte-selective enhancement is characterized by bile accumulation in tumors.

References

1. Bluemke DA, Sahani D, Amendola M, et al. Efficacy and safety of MR imaging with liver-specific contrast agent: U.S. multicenter phase III study. Radiology 2005;237(1):89–98.
2. Vogl TJ, Kümmel S, Hammerstingl R, et al. Liver tumors: comparison of MR imaging with Gd-EOB-DTPA and Gd-DTPA. Radiology 1996;200(1):59–67.
3. Bartolozzi C, Crocetti L, Lencioni R, Cioni D, Della Pina C, Campani D. Biliary and reticuloendothelial impairment in hepatocarcinogenesis: the diagnostic role of tissue-specific MR contrast media. Eur Radiol 2007;17(10):2519–2530.
4. Hamm B, Staks T, Mühler A, et al. Phase I clinical evaluation of Gd-EOB-DTPA as a hepatobiliary MR contrast agent: safety, pharmacokinetics, and MR imaging. Radiology 1995;195(3):785–792.
5. Huppertz A, Balzer T, Blakeborough A, et al. Improved detection of focal liver lesions at MR imaging: multicenter comparison of gadoxetic acid-enhanced MR images with intraoperative findings. Radiology 2004;230(1):266–275.
6. Reimer P, Rummeny EJ, Daldrup HE, et al. Enhancement characteristics of liver metastases, hepatocellular carcinomas, and hemangiomas with Gd-EOB-DTPA: preliminary results with dynamic MR imaging. Eur Radiol 1997;7(2):275–280.
7. Kim SH, Kim SH, Lee J, et al. Gadoxetic acid-enhanced MRI versus triple-phase

MDCT for the preoperative detection of hepatocellular carcinoma. AJR Am J Roentgenol 2009;192(6):1675–1681.

8. Huppertz A, Haraida S, Kraus A, et al. Enhancement of focal liver lesions at gadoxetic acid-enhanced MR imaging: correlation with histopathologic findings and spiral CT—initial observations. Radiology 2005;234(2):468–478.
9. Zech CJ, Grazioli L, Breuer J, Reiser MF, Schoenberg SO. Diagnostic performance and description of morphological features of focal nodular hyperplasia in Gd-EOB-DTPA-enhanced liver magnetic resonance imaging: results of a multicenter trial. Invest Radiol 2008;43(7):504–511.
10. Narita M, Hatano E, Arizono S, et al. Expression of OATP1B3 determines uptake of Gd-EOB-DTPA in hepatocellular carcinoma. J Gastroenterol 2009;44(7):793–798.
11. Ni Y, Marchal G, Yu J, Mühler A, Lukito G, Baert AL. Prolonged positive contrast enhancement with Gd-EOB-DTPA in experimental liver tumors: potential value in tissue characterization. J Magn Reson Imaging 1994;4(3):355–363.
12. Fujita M, Yamamoto R, Fritz-Zieroth B, et al. Contrast enhancement with Gd-EOB-DTPA in MR imaging of hepatocellular carcinoma in mice: a comparison with superparamagnetic iron oxide. J Magn Reson Imaging 1996;6(3):472–477.
13. Clément O, Mühler A, Vexler V, Berthezène Y, Brasch RC. Gadolinium-ethoxybenzyl-DTPA, a new liver-specific magnetic resonance contrast agent: kinetic and enhancement patterns in normal and cholestatic rats. Invest Radiol 1992;27(8):612–619.
14. Pascolo L, Petrovic S, Cupelli F, et al. Abc protein transport of MRI contrast agents in canalicular rat liver plasma vesicles and yeast vacuoles. Biochem Biophys Res Commun 2001;282(1):60–66.
15. van Montfoort JE, Stieger B, Meijer DK, Weinmann HJ, Meier PJ, Fattinger KE. Hepatic uptake of the magnetic resonance imaging contrast agent gadoxetate by the organic anion transporting polypeptide Oatp1. J Pharmacol Exp Ther 1999;290(1):153–157.
16. König J, Cui Y, Nies AT, Keppler D. A novel human organic anion transporting polypeptide localized to the basolateral hepatocyte membrane. Am J Physiol Gastrointest Liver Physiol 2000;278(1):G156–G164.
17. König J, Cui Y, Nies AT, Keppler D. Localization and genomic organization of a new hepatocellular organic anion transporting polypeptide. J Biol Chem 2000;275(30):23161–23168.
18. Vander Borght S, Libbrecht L, Blokzijl H, et al. Diagnostic and pathogenetic implications of the expression of hepatic transporters in focal lesions occurring in normal liver. J Pathol 2005;207(4):471–482.
19. Cui Y, König J, Nies AT, et al. Detection of the human organic anion transporters SLC21A6 (OATP2) and SLC21A8 (OATP8) in liver and hepatocellular carcinoma. Lab Invest 2003;83(4):527–538.
20. Zollner G, Wagner M, Fickert P, et al. Hepatobiliary transporter expression in human hepatocellular carcinoma. Liver Int 2005;25(2):367–379.
21. Vavricka SR, Jung D, Fried M, Grützner U, Meier PJ, Kullak-Ublick GA. The human organic anion transporting polypeptide 8 (SLCO1B3) gene is transcriptionally repressed by hepatocyte nuclear factor 3β in hepatocellular carcinoma. J Hepatol 2004;40(2):212–218.
22. Nies AT, König J, Pfannschmidt M, Klar E, Hofmann WJ, Keppler D. Expression of the multidrug resistance proteins MRP2 and MRP3 in human hepatocellular carcinoma. Int J Cancer 2001;94(4):492–499.
23. International Consensus Group for Hepatocellular Neoplasia. Pathologic diagnosis of early hepatocellular carcinoma: a report of the International Consensus Group for Hepatocellular Neoplasia. Hepatology 2009;49(2):658–664.
24. Liver Cancer Study Group of Japan. The general rules for the clinical and pathological study of primary liver cancer. Tokyo, Japan: Kanehara, 2008.
25. Edmondson HA, Steiner PE. Primary carcinoma of the liver: a study of 100 cases among 48,900 necropsies. Cancer 1954;7(3):462–503.
26. Imai Y, Murakami T, Yoshida S, et al. Superparamagnetic iron oxide-enhanced magnetic resonance images of hepatocellular carcinoma: correlation with histological grading. Hepatology 2000;32(2):205–212.
27. Ueda K, Terada T, Nakanuma Y, Matsui O. Vascular supply in adenomatous hyperplasia of the liver and hepatocellular carcinoma: a morphometric study. Hum Pathol 1992;23(6):619–626.
28. Honda H, Tajima T, Kajiyama K, et al. Vascular changes in hepatocellular carcinoma: correlation of radiologic and pathologic findings. AJR Am J Roentgenol 1999;173(5):1213–1217.
29. Burt AD, Portmann BC, Ferrel LD. MacSween's pathology of the liver. 5th ed. London, England: Churchill Livingstone, 2006.
30. Cui Y, König J, Leier I, Buchholz U, Keppler D. Hepatic uptake of bilirubin and its conjugates by the human organic anion transporter SLC21A6. J Biol Chem 2001;276(13):9626–9630.
31. Kamisako T, Leier I, Cui Y, et al. Transport of monoglucuronosyl and bisglucuronosyl bilirubin by recombinant human and rat multidrug resistance protein 2. Hepatology 1999;30(2):485–490.
32. Nilsson H, Nordell A, Vargas R, Douglas L, Jonas E, Blomqvist L. Assessment of hepatic extraction fraction and input relative blood flow using dynamic hepatocyte-specific contrast-enhanced MRI. J Magn Reson Imaging 2009;29(6):1323–1331.
33. Pauli-Magnus C, Meier PJ. Hepatobiliary transporters and drug-induced cholestasis. Hepatology 2006;44(4):778–787.